Scholars Journal of Engineering and Technology

OPEN ACCESS

Abbreviated Key Title: Sch J Eng Tech
ISSN 2347-9523 (Print) | ISSN 2321-435X (Online)
Journal homepage: https://saspublishers.com

Aloe vera Phytochemical-Mediated Synthesis of ZnO Nanoparticles: Zn^{2+} Complexation, Controlled Alkaline Precipitation, Surface Capping, and Calcination-Induced Wurtzite Crystallization

Altaf Hussain[1], Shariq Hassan[2]*, Salma Parveen[3], Muhammad Zubair Mehboob[4], Khan Arbaz Ali[5], Shahzad Ahmad[3], Abdur Rahman[6], Nabeel Tariq[7]

[1]Institute of Physics, The Islamia University of Bahawalpur, Punjab 63100, Pakistan
[2]Department of Chemistry, University of Agriculture, Faisalabad, Pakistan
[3]Centre of Excellence in Solid State Physics, University of the Punjab, Lahore, Pakistan
[4]Department of Chemistry, Government College University Lahore, Lahore, Punjab 54000, Pakistan
[5]Institute of Molecular Biology and Biotechnology, The University of Lahore, Lahore, Pakistan
[6]Department of Chemical and Life Sciences, Qurtuba University of Science and Technology, Peshawar, Khyber Pakhtunkhwa, Pakistan
[7]Department of Physics, University of Sargodha, Sargodha 40100, Punjab, Pakistan

DOI: https://doi.org/10.36347/sjet.2026.v14i09.003 | **Received:** 25.07.2026 | **Accepted:** 14.09.2026 | **Published:** 16.09.2026

***Corresponding author:** Shariq Hassan
Department of Chemistry, University of Agriculture, Faisalabad, Pakistan

Abstract | **Original Research Article**

Plant-assisted synthesis offers a lower-hazard route to zinc oxide (ZnO) nanomaterials, yet the amount of plant extract can simultaneously alter nucleation, crystal growth, surface passivation, aggregation, and optical response. In this study, ZnO powders were prepared by alkaline precipitation from zinc acetate using 0, 10, 15, 20, 25, and 30 mL of Aloe vera inner-leaf gel extract, followed by drying and calcination at 350 °C. The extract is interpreted principally as a phytochemical complexing, growth-regulating, and surface-capping medium rather than as a conventional reducing reagent for Zn(II). X-ray diffraction patterns were consistent with hexagonal wurtzite ZnO and did not show obvious additional crystalline phases within the reported scans. Among the concentration series, the 15 mL sample exhibited the highest reported (selected-peak) intensity (2067 a.u.), the lowest full width at half maximum (0.49327°), the largest Scherrer crystallite size (17.05 nm), and the lowest single-line microstrain estimate (0.00620), indicating the most ordered structure under the tested conditions. Fourier-transform infrared spectra contained Zn-O absorption in the approximately 448-600 cm^{-1} region together with O-H, C-H, C-O, and carbonyl/amide-related bands consistent with residual Aloe-derived surface species. UV-visible absorption edges occurred in the near-UV region, while near-band-edge photoluminescence at 378-392 nm corresponded to photon energies of approximately 3.16-3.29 eV. By contrast, concentration-series Tauc intercepts of 5.6-6.2 eV were physically inconsistent with the absorption edges and photoluminescence and are therefore reported only as apparent values requiring recalculation from raw, baseline-corrected spectra. Overall, 15 mL provided the most balanced structural and surface response in the available dataset. Morphology, composition, colloidal stability, replicate synthesis, uncertainty analysis, and application-specific performance remain necessary before technological claims can be validated.

Keywords: zinc oxide nanoparticles; Aloe vera; green precipitation; phytochemical capping; extract concentration; X-ray diffraction; optical band gap; photoluminescence.

1. INTRODUCTION

1.1 ZnO as a multifunctional semiconductor

Zinc oxide is a II-VI semiconductor that crystallizes most commonly in the hexagonal wurtzite structure. Its direct near-UV band gap, comparatively large exciton binding energy, chemical robustness, and accessible surface chemistry have made ZnO relevant to ultraviolet emitters and detectors, transparent and flexible electronics, gas and biosensors, photocatalysis, antimicrobial materials, and interfacial layers in energy devices [1,2]. At the nanoscale, these functions are strongly influenced by crystallite size, morphology,

exposed facets, surface hydroxylation, native defects, adsorbed species, and particle-particle aggregation. Therefore, a synthesis variable that appears simple—such as the amount of plant extract—can alter several material properties at the same time.

Conventional sol-gel, hydrothermal, vapor-phase, microwave-assisted, and precipitation routes can provide good control over ZnO morphology and crystallinity, but some protocols use hazardous ligands or solvents, require elevated pressure, or generate waste streams that are difficult to manage. Plant-assisted precipitation is attractive because aqueous extracts can supply hydroxyl-, carbonyl-, carboxyl-, and polysaccharide-rich molecules that interact with zinc-containing precursor species and newly formed oxide surfaces [2-4]. The environmental benefit, however, depends on the whole process—including precursor choice, water and energy use, pH adjustment, washing, calcination, yield, and waste treatment—not merely on the biological origin of the extract.

1.2 Chemical role of Aloe vera inner-leaf gel

Aloe vera inner-leaf gel is predominantly water but contains polysaccharides, soluble sugars, proteins, amino acids, minerals, enzymes, and minor phenolic constituents. Acemannan- and glucomannan-type polysaccharides are frequently emphasized in compositional studies of the gel [5]. In an alkaline zinc-acetate system, these molecules can coordinate Zn(II), influence local supersaturation, adsorb on growing ZnO surfaces, and leave a carbonaceous or oxygenated surface residue after drying. The term "green synthesis" should therefore not be interpreted as proof of a single reduction mechanism. Unlike metallic nanoparticle formation, Zn remains in the +2 oxidation state during conversion from zinc salt/hydroxide intermediates to ZnO; the extract is more defensibly described as a complexing, nucleation-modulating, growth-directing, and capping medium.

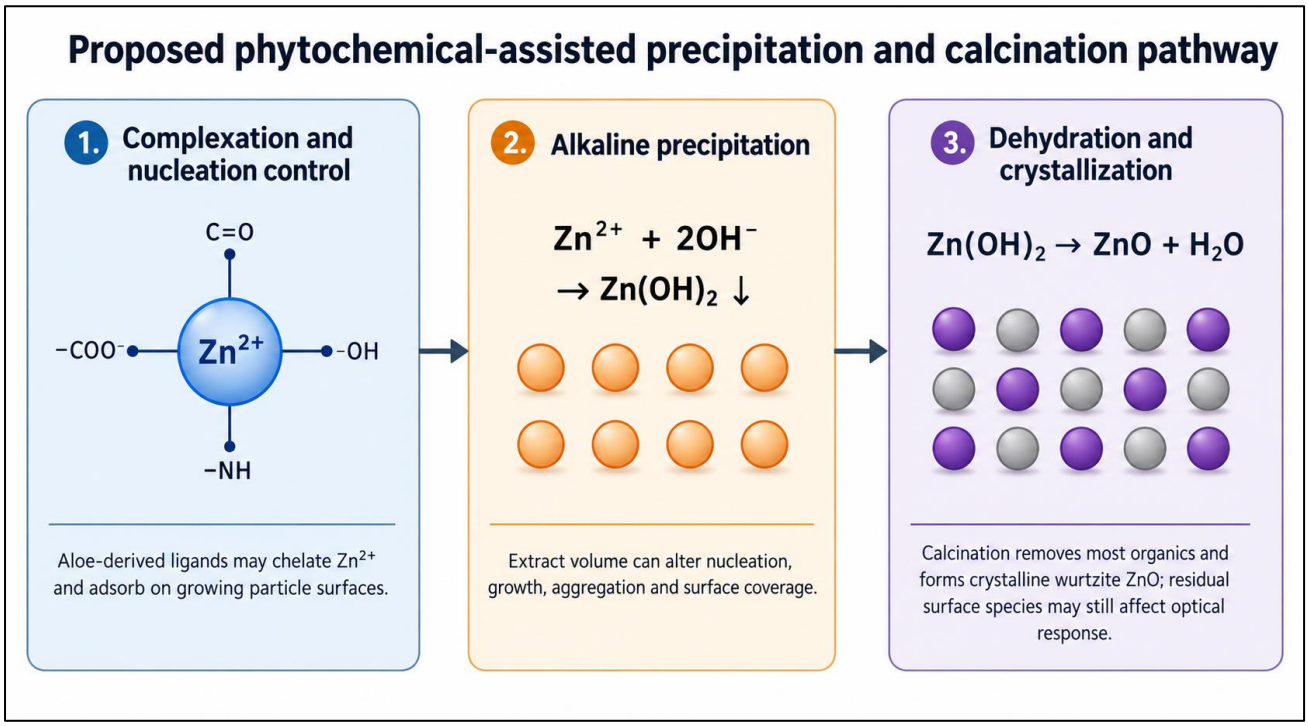

Figure 1: Proposed physicochemical pathway for Aloe vera-assisted ZnO precipitation. The diagram is a literature-grounded mechanistic model, not direct evidence of specific molecular binding in the present samples

1.3 Research gap, hypothesis, and study objective

Aloe vera-mediated ZnO has been reported previously, including comparative chemical/biological synthesis and studies of optical and functional behavior [3,4]. Nevertheless, extract concentration is often treated as a procedural detail rather than an independent variable. Too little extract may provide incomplete surface coverage; an intermediate amount may balance nucleation and growth; and excess organic matter may increase viscosity, alter local pH, obstruct crystallization, or promote secondary aggregation during drying and calcination. These competing effects predict a non-monotonic concentration-response rather than a simple linear trend.

The present study therefore evaluates how Aloe vera inner-gel extract volume (10-30 mL) changes the XRD, FTIR, UV-visible, and photoluminescence signatures of precipitated ZnO relative to an uncapped control. The working hypothesis is that an intermediate extract volume provides the most favorable compromise between structural order and phytochemical surface stabilization. A second objective of this revision is to critically reconcile the different optical-energy estimates and to distinguish conclusions supported by the supplied

measurements from claims that require additional characterization.

2. MATERIALS AND METHODS

2.1 Materials

Zinc acetate dihydrate ($Zn(CH_3COO)_2 \cdot 2H_2O$, >98.5%), sodium hydroxide, ethanol (>99%), deionized water, and fresh Aloe vera leaves were used. The grade, supplier, lot number, and storage conditions of every reagent should be added to the final submission because precursor impurities and water quality can influence nucleation and optical spectra.

2.2 Preparation of Aloe vera inner-gel extract

Fresh leaves were washed thoroughly. The outer rind and latex-rich layer were removed, and 25 g of the transparent inner gel was collected. The gel was dispersed in 100 mL of distilled water, heated at 80 °C for 20 min with continuous stirring, cooled to room temperature, and filtered to obtain the working extract. For reproducibility, future experiments should additionally report plant age or source, leaf position, time from harvesting to extraction, extract pH, dry-solids content, filtration pore size, and storage time. These parameters can change the concentration of soluble macromolecules and phenolic constituents.

2.3 ZnO precipitation and extract-concentration design

A 0.4 M zinc acetate solution was mixed with 0, 10, 15, 20, 25, or 30 mL of the prepared Aloe vera extract and maintained at 80 °C under magnetic stirring. A 0.5 M NaOH solution was added dropwise until pH 9 was reached, after which stirring continued for 2 h. The white precipitate was collected by centrifugation, repeatedly washed with deionized water and ethanol, dried at 80 °C overnight, and calcined at 350 °C for 2 h. All conditions other than extract volume were intended to remain constant.

$$Zn^{2+} + 2OH^- \rightarrow Zn(OH)_2 \rightarrow ZnO + H_2O$$

Simplified precipitation/dehydration pathway; zinc remains in the +2 oxidation state.

Reproducibility requirement: The final paper should report total reaction volume, NaOH addition rate, stirring speed, centrifugation force and time, number of washes, heating/cooling rates, crucible type, sample mass per crucible, and product yield. At least three independently prepared batches per condition are needed for defensible statistical comparison.

2.4 Characterization

X-ray diffraction (XRD) was used to examine crystalline phase, peak position, peak width, and relative intensity. Fourier-transform infrared (FTIR) spectroscopy was used to identify Zn-O vibrations and residual organic functional groups. UV-visible spectroscopy was used to locate absorption-edge behavior and construct direct-transition Tauc representations. Photoluminescence (PL) spectroscopy, recorded with 330 nm excitation over approximately 350-500 nm, was used to compare near-band-edge and visible-emission features. Instrument manufacturer/ model, scan range, step size, dwell time, slit configuration, sample preparation, spectral resolution, path length or diffuse-reflectance geometry, blank/reference procedure, and replicate count were not provided in the source manuscript and must be reported before journal submission.

2.5 Structural and optical calculations

Crystallite size may be estimated from peak broadening using the Scherrer relation, provided that β is the instrument-corrected full width at half maximum in radians and that the selected reflection is not strongly affected by overlap or anisotropic broadening:

$$D = K\lambda / (\beta \cos\theta)$$

D is coherent-domain size, K is the shape factor (commonly ~0.9), λ is the X-ray wavelength, β is corrected FWHM, and θ is the Bragg angle.

Interplanar spacing follows Bragg's law. For wurtzite ZnO, lattice parameters should be refined from several indexed reflections rather than calculated from a single mixed-index peak:

$$n\lambda = 2d \sin\theta$$

$$1/d^2 = (4/3)(h^2 + hk + k^2)/a^2 + l^2/c^2$$

A one-peak line-broadening strain proxy is sometimes written as $\varepsilon \approx \beta/(4 \tan\theta)$. It is not a full Williamson-Hall analysis. A true Williamson-Hall treatment requires several diffraction peaks and a regression of $\beta\cos\theta$ against $4\sin\theta$, ideally after instrumental broadening correction.

$$\varepsilon \approx \beta / (4 \tan\theta)$$

Reported here only as a single-line estimate because multi-peak regression data were not supplied.

For a direct allowed transition, a Tauc representation is commonly written as $(\alpha h\nu)^2$ versus $h\nu$. Reliable extraction requires a physically meaningful absorption coefficient (or an appropriate Kubelka-Munk treatment for diffuse reflectance), baseline correction, a justified linear fitting interval, and uncertainty assessment [6-8].

$$(\alpha h\nu)^2 = A(h\nu - E_g)$$

2.6 Data interpretation and transparency

The current dataset is descriptive: means, standard deviations, independent replicate syntheses, and inferential tests were not supplied. Consequently, terms such as "significant" are avoided unless statistical testing is later performed. Values transcribed from plots are

treated as reported observations rather than exact metrological results. Where independent indicators disagree, the disagreement is discussed explicitly instead of selecting only the value that supports the preferred interpretation.

3. RESULTS AND DISCUSSION

3.1 Capped versus uncapped ZnO: structural comparison

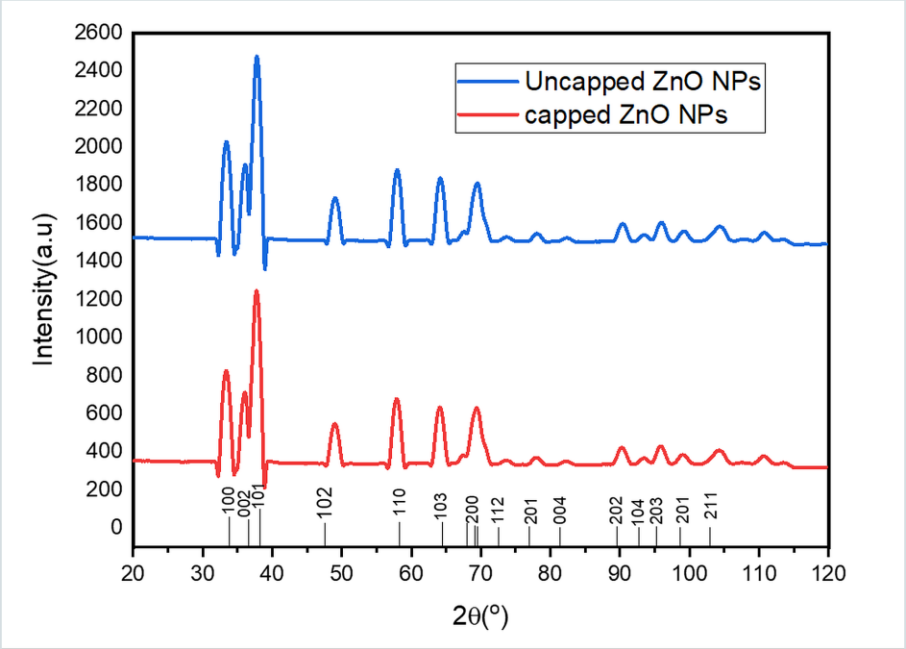

Figure 2. XRD patterns of uncapped and Aloe vera-capped ZnO.

The diffraction patterns contain the characteristic set of reflections expected for wurtzite ZnO. The absence of conspicuous additional peaks is consistent with a predominantly ZnO crystalline phase, but it does not prove absolute phase purity because amorphous material, low-concentration impurities, and overlapping phases may remain undetected. Reference powder data for wurtzite ZnO give lattice constants near a = 3.25 Å and c = 5.21 Å and place the strong (100), (002), and (101) reflections in the low-30° to mid-30° 2θ range for Cu Kα radiation [9].

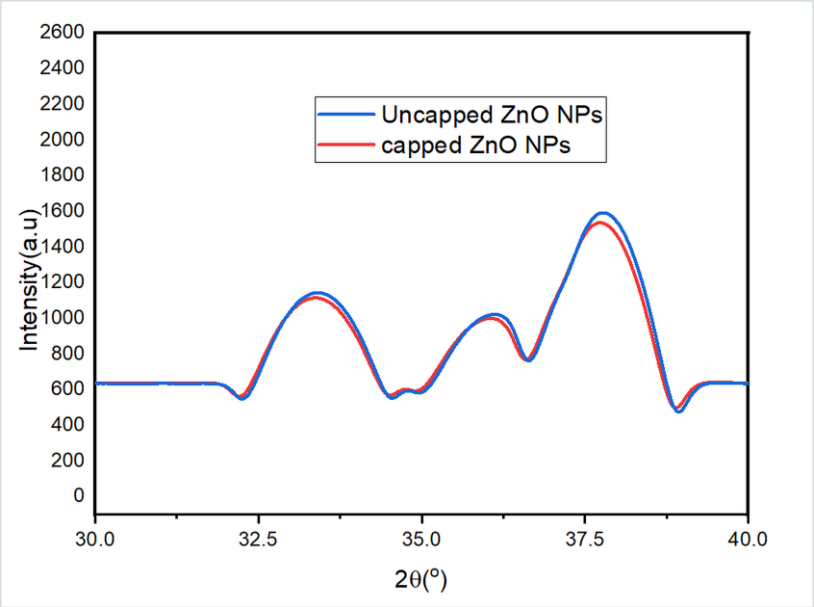

Figure 3: Expanded XRD region comparing selected peaks of capped and uncapped samples

The manuscript originally associated a lower capped-sample peak intensity with inhibited crystal growth and surface binding by phytochemicals. That interpretation is plausible but not unique: peak height can

also change because of sample packing, preferred orientation, background subtraction, instrumental alignment, or vertical normalization. Peak width, integrated area, and replicate measurements provide a more robust structural comparison than peak height alone.

Sample	Plane	2θ (°)	FWHM (°)	Recalculated D (nm)	Reported d (Å)	Structurally consistent parameter
Uncapped	(002)	34.4	1.28125	6.54	2.60	c ≈ 5.20 Å
Uncapped	(101)	36.2	1.28126	6.63	2.47	Requires multi-peak refinement
Capped	(002)	34.4	1.28126	6.54	2.60	c ≈ 5.20 Å
Capped	(101)	36.2	1.28126	6.63	2.47	Requires multi-peak refinement

Note. Scherrer sizes were recalculated from the FWHM and 2θ values reported in the source manuscript using K = 0.9 and Cu Kα λ = 0.15406 nm. The original 65.53 nm value is inconsistent with FWHM = 1.28125° and appears to contain a decimal-place error. Instrumental broadening was not available, so these values are approximate.

XRD correction: The reported d(002) = 2.60 Å implies c = 2d = 5.20 Å, not 4.76 Å. Also, a = 2.75 Å is below the accepted wurtzite ZnO value and should not be retained without re-indexing and full-pattern refinement.

3.2 FTIR evidence for ZnO formation and phytochemical association

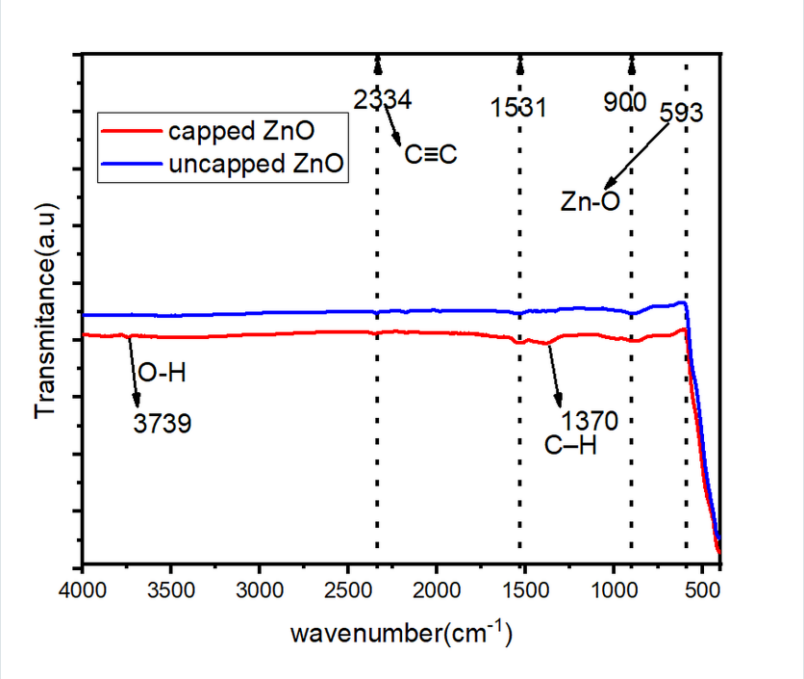

Figure 4: FTIR spectra of capped and uncapped ZnO

Both spectra show strong low-wavenumber absorption attributable to Zn-O lattice vibrations, while the capped sample displays additional or stronger features assigned to O-H, C-H, C-O, carbonyl/amide, and aromatic or unsaturated organic groups. These bands are compatible with residual polysaccharide-, protein-, and phenolic-derived material from Aloe vera on the particle surface. The broad O-H region can also contain physically adsorbed water and surface hydroxyl groups, and the approximately 2330-2360 cm^{-1} feature can include atmospheric CO_2. Therefore, FTIR supports surface association but does not identify a unique capping molecule or prove a specific coordination geometry.

The original assignment of a 2334 cm^{-1} feature exclusively to C≡C stretching should be treated cautiously because ambient CO_2 and instrumental background are common contributors in this region. Similarly, bands near 1500-1650 cm^{-1} may contain overlapping water bending, amide, aromatic C=C, and carboxylate modes. Comparison with a spectrum of the dried extract and with the calcined blank would strengthen the interpretation.

3.3 UV-visible response and band-gap consistency

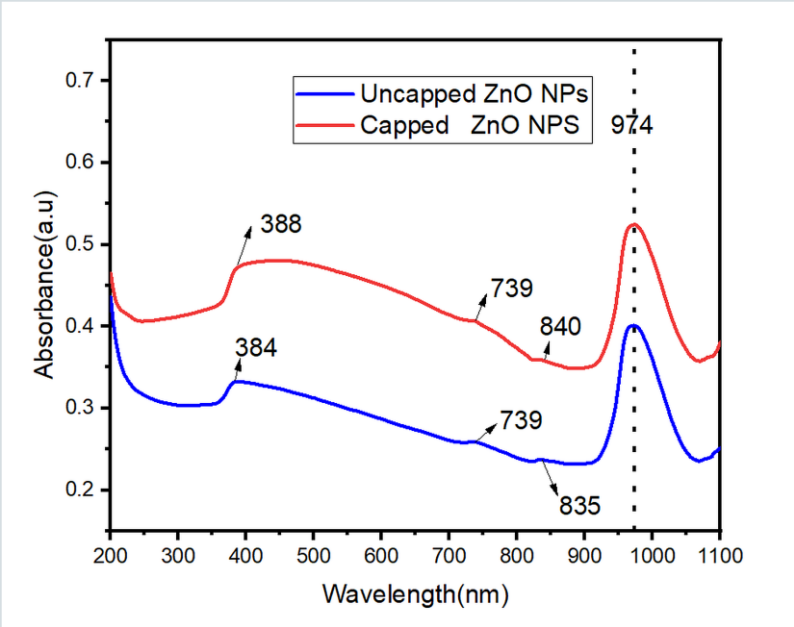

Figure 5: UV-visible absorbance spectra of capped and uncapped ZnO

The principal absorption edges near 384-388 nm are consistent with near-UV interband absorption in ZnO. A wavelength-to-energy conversion, E(eV) = 1240/λ(nm), gives approximately 3.23 eV at 384 nm and 3.20 eV at 388 nm. These values align with the expected ZnO optical regime and with the near-band-edge PL positions. The broad features reported near 739-974 nm are not typical intrinsic ZnO band-edge absorption and should not automatically be assigned to oxygen vacancies. Particle scattering, agglomeration, baseline drift, optical-path changes, or detector/grating transitions must first be excluded.

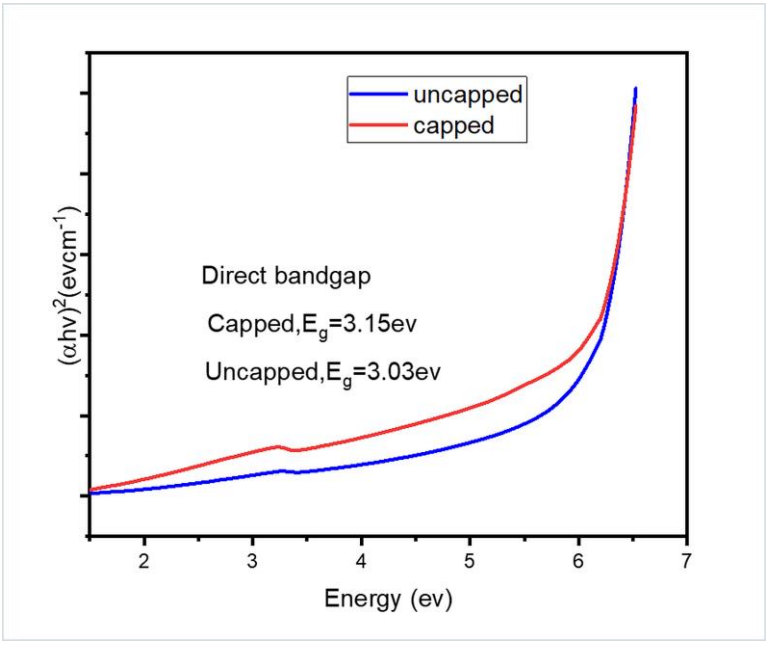

Figure 6: Direct-transition Tauc representation for capped and uncapped ZnO

The capped/uncapped Tauc plot gives intercepts of 3.03 and 3.15 eV, which are broadly plausible for nanocrystalline ZnO, although they are lower than the simple absorption-edge energies. Such differences can arise from band tails, defect absorption, scattering, and subjective selection of the fitted region. Best practice requires showing the original spectrum, the transformation used to calculate α or F(R), the selected linear interval, the fitted equation and coefficient of determination, and confidence intervals [6-8].

3.4 Photoluminescence and defect-sensitive emission

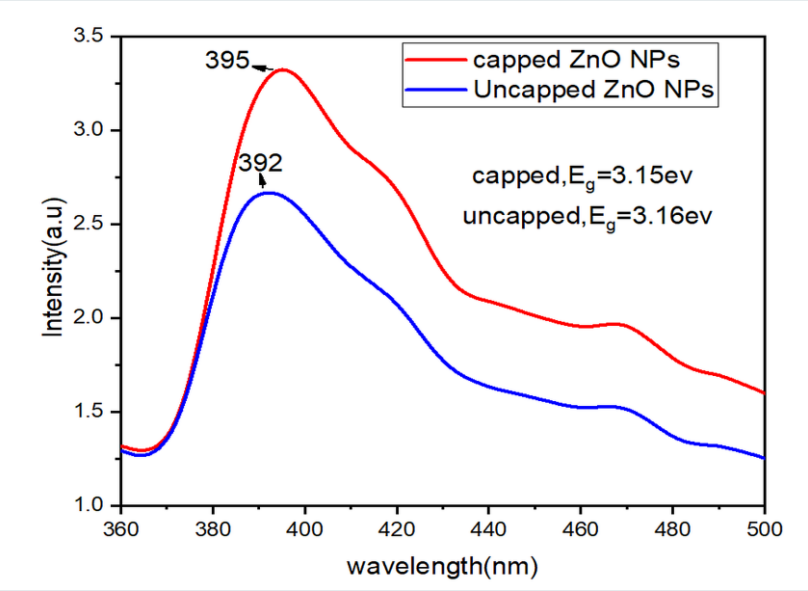

Figure 7: PL spectra of capped and uncapped ZnO at 330 nm excitation

Near-band-edge peaks at 392 nm (uncapped) and 395 nm (capped) correspond to approximately 3.16 and 3.14 eV, respectively. The capped spectrum shows greater intensity in the plotted comparison. This can be consistent with reduced non-radiative surface trapping, but PL intensity is not a direct standalone measure of "fewer defects": it can also vary with particle concentration, absorption at the excitation wavelength, scattering, packing, instrument settings, and the balance between radiative and non-radiative pathways.

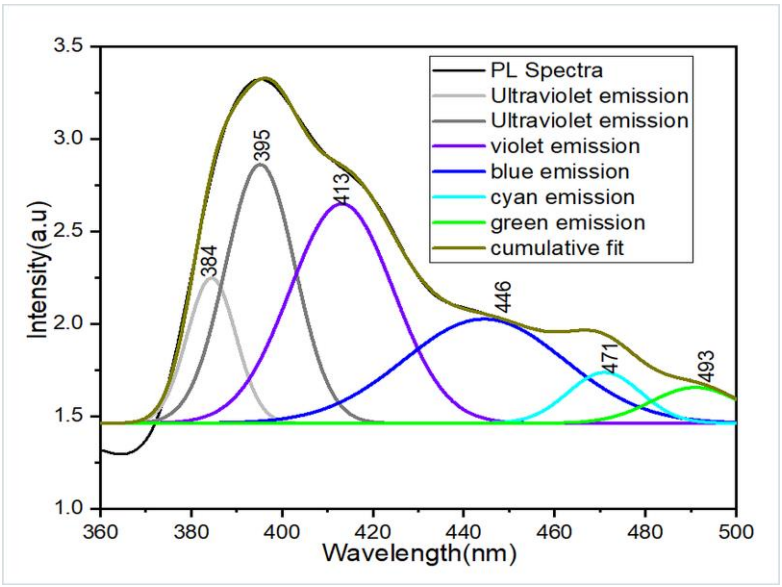

Figure 8: Gaussian component representation of the capped-ZnO PL spectrum

The deconvolution contains components near 384, 395, 413, 446, 471, and 493 nm. Near-UV components can be described as excitonic or near-band-edge emission. Visible components are defect- and surface-sensitive, but assigning each peak uniquely to a specific oxygen vacancy or zinc interstitial is not justified by room-temperature PL alone. ZnO green and blue luminescence has multiple proposed origins—including impurities, zinc vacancies, oxygen-related defects, and surface states—and the literature does not support a universal one-peak/one-defect mapping [10]. Temperature-dependent PL, excitation spectra, time-resolved PL, electron paramagnetic resonance, and controlled-atmosphere annealing would be needed for stronger defect identification.

3.5 Effect of Aloe vera extract concentration on XRD response

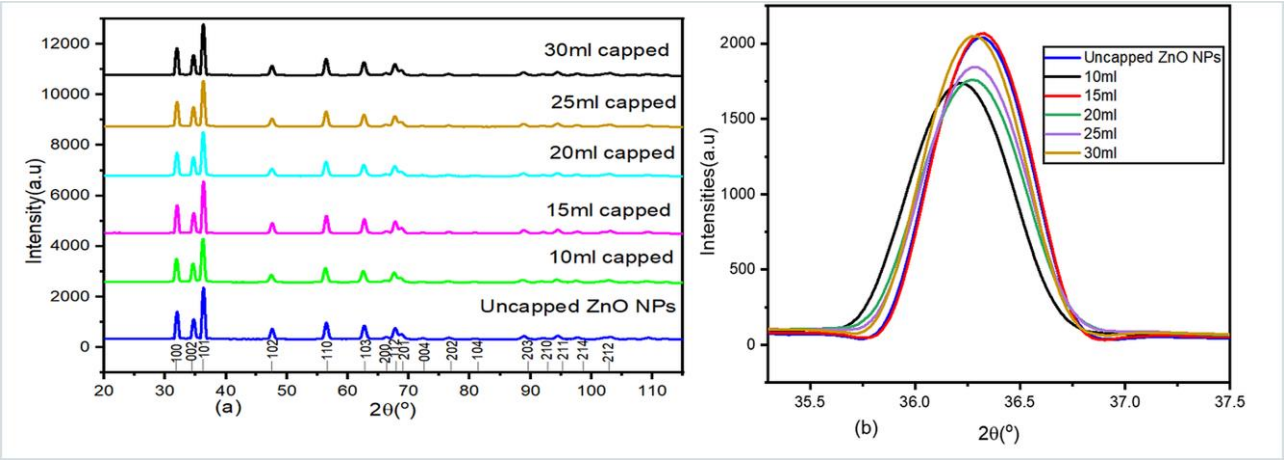

Figure 9: XRD patterns across the 0-30 mL extract series and expanded selected-peak region

All concentration-series patterns retain a similar ZnO-like reflection set, suggesting that extract volume did not produce an obvious new crystalline phase. The selected peak intensity followed a non-monotonic trend: 2033 a.u. (0 mL), 1731 a.u. (10 mL), 2067 a.u. (15 mL), 1761 a.u. (20 mL), 1844 a.u. (25 mL), and 2055 a.u. (30 mL). The 15 mL sample therefore gave the highest reported value, but the 30 mL result was similar. Without replicate scans, integrated peak areas, and normalization to sample mass or an internal standard, the small difference between 15 and 30 mL should not be overstated.

Extract (mL)	Reported 2θ (°)	FWHM (°)	Scherrer D (nm)	Selected-peak intensity (a.u.)
0	38.28525	0.50162	16.76	2033
10	38.18740	0.54511	15.42	1731
15	38.29072	0.49327	17.05	2067
20	38.24262	0.54508	15.42	1761
25	38.25607	0.52875	15.90	1844
30	38.25270	0.50688	16.59	2055

Note. Values are transcribed from the supplied manuscript. The peak was reported as (101), but standard Cu Kα wurtzite ZnO places (101) near 36.25°, not ~38.2°. Raw XRD files, wavelength, and indexing must be verified before publication.

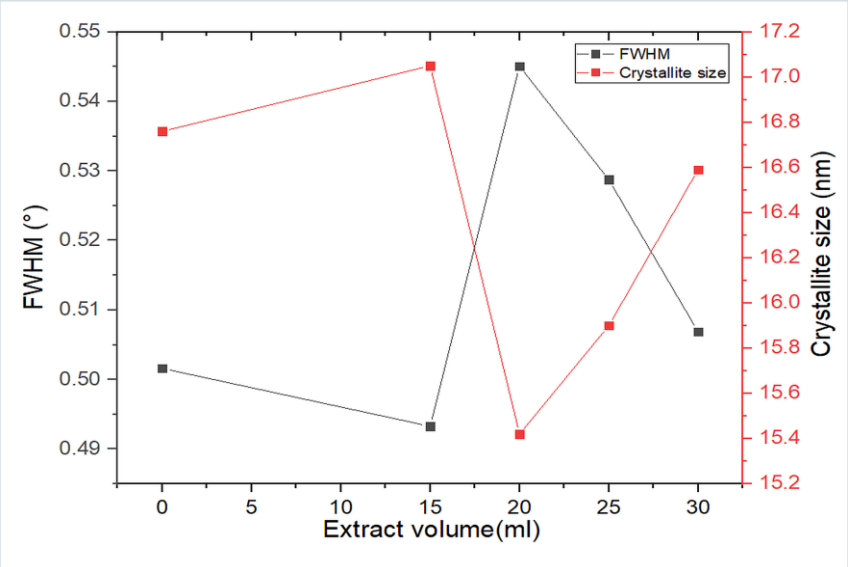

Figure 10: Reported FWHM and Scherrer crystallite-size response to extract volume

FWHM and Scherrer size show the expected inverse mathematical relationship because the same line width is used in the size calculation. The 15 mL sample combines the lowest reported FWHM (0.49327°) with the largest calculated coherent-domain size (17.05 nm). This supports improved structural order at that condition

within the limits of the selected peak. The 10 and 20 mL samples have the broadest peaks and smallest domains, whereas the 25 and 30 mL samples partially recover. The zigzag trend is consistent with competition among complexation, nucleation, surface adsorption, drying-induced aggregation, and calcination, but these mechanisms cannot be separated by XRD alone.

3.6 Single-line microstrain estimate

Extract (mL)	FWHM (°)	β (rad)	Reported d (Å)	Reported ε
10	0.54511	0.00951	2.3800	0.00685
15	0.49327	0.00861	2.3800	0.00620
20	0.54508	0.00951	2.3800	0.00685
25	0.52875	0.00923	2.3800	0.00665
30	0.50688	0.00885	2.3800	0.00638

Note. These values are single-line strain proxies calculated from the reported selected peak. They should not be labeled a Williamson-Hall analysis because no multi-peak regression was presented.

The minimum reported strain proxy at 15 mL (0.00620) is internally consistent with that sample's narrowest peak and largest Scherrer domain. However, because both size and strain were derived from the same FWHM, their apparent agreement is partly mathematical rather than independent confirmation. A defensible separation of size and strain broadening requires several reflections, instrumental correction, and a Williamson-Hall or more advanced line-profile model.

3.7 Concentration-dependent FTIR surface chemistry

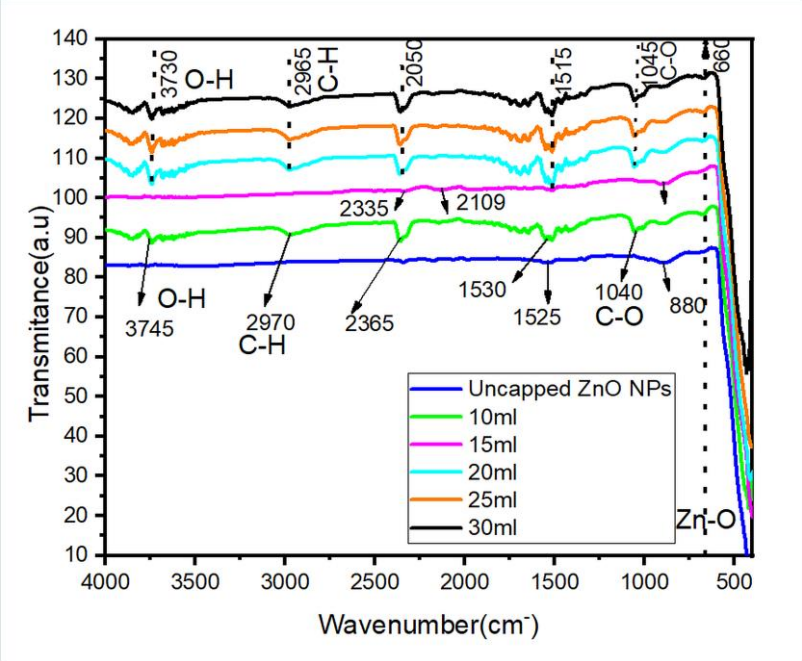

Figure 11: FTIR spectra of uncapped ZnO and the 10-30 mL extract series

The concentration series retains the low-wavenumber Zn-O region and displays varying O-H, C-H, C-O, and carbonyl/amide-related features. Increasing extract volume can increase the quantity or composition of organic species that reach the oxide surface, but peak height in stacked FTIR spectra is not automatically proportional to surface coverage because sample mass, pellet thickness, ATR contact, baseline, and normalization also matter. The 15 mL sample was described as showing balanced organic and Zn-O features; this qualitative interpretation should be supported by normalized spectra and integrated band areas if the authors wish to compare capping quantitatively.

Thermogravimetric analysis coupled with mass spectrometry or FTIR, X-ray photoelectron spectroscopy, total organic carbon, and zeta-potential measurements would provide more direct evidence of residual organic coverage and surface chemistry after calcination. An FTIR spectrum of the dried Aloe extract and of ZnO prepared without calcination would help distinguish molecular adsorption from thermally transformed residues.

3.8 Concentration-dependent optical absorption: resolving an internal inconsistency

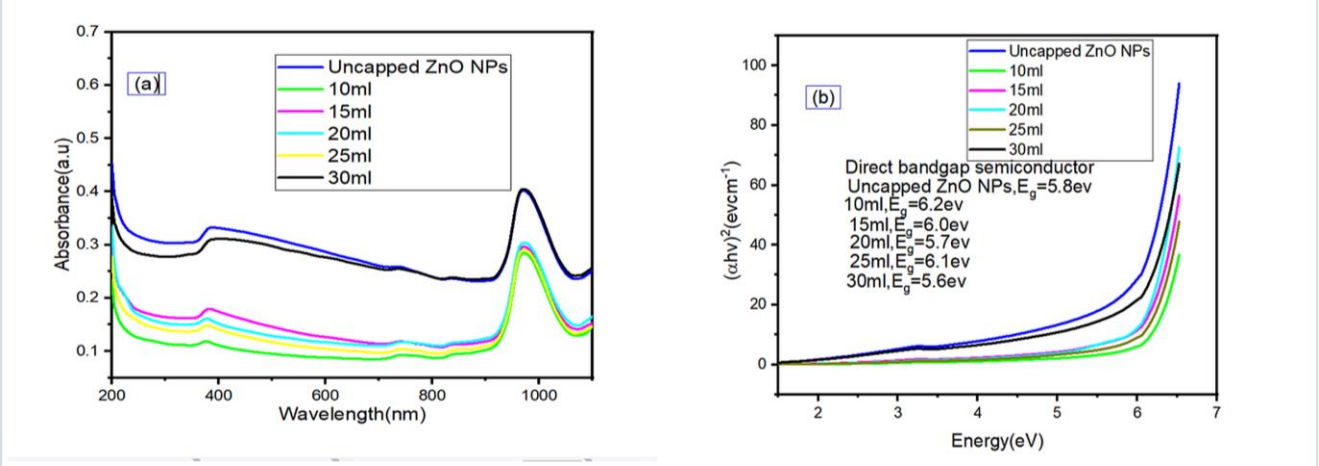

Figure 12: UV-visible spectra and corresponding concentration-series Tauc representations

The spectra show near-UV edge behavior around 370-400 nm, which corresponds approximately to 3.10-3.35 eV. The source manuscript, however, labels Tauc intercepts of 5.8 eV (0 mL), 6.2 eV (10 mL), 6.0 eV (15 mL), 5.7 eV (20 mL), 6.1 eV (25 mL), and 5.6 eV (30 mL). A 6.0 eV transition corresponds to about 207 nm, which is incompatible with assigning a 370-400 nm edge as the same fundamental ZnO band gap. Crystallite sizes of approximately 15-17 nm are also too large to justify such an extreme quantum-confinement shift for ZnO.

Analytical caution: The 5.6-6.2 eV numbers should not be presented as intrinsic ZnO band gaps. They are retained only as "apparent Tauc intercepts" to preserve transparency. Recalculate E_g from exported raw spectra after blank subtraction, baseline/scattering treatment, conversion to α or Kubelka-Munk function as appropriate, and objective linear-region selection.

Extract (mL)	Apparent Tauc intercept (eV)	PL/edge-compatible energy (eV)	Interpretation
0	5.8	≈3.16-3.23	Tauc value not physically consistent
10	6.2	≈3.29	Tauc value not physically consistent
15	6.0	≈3.24	Tauc value not physically consistent
20	5.7	≈3.25	Tauc value not physically consistent
25	6.1	≈3.25	Tauc value not physically consistent
30	5.6	≈3.16	Tauc value not physically consistent

Note. The ~3.16-3.29 eV values are based on the near-band-edge PL labels and/or near-UV absorption positions shown in the supplied figures. They are not a substitute for a properly recalculated optical band gap with uncertainty.

3.9 Concentration-dependent photoluminescence

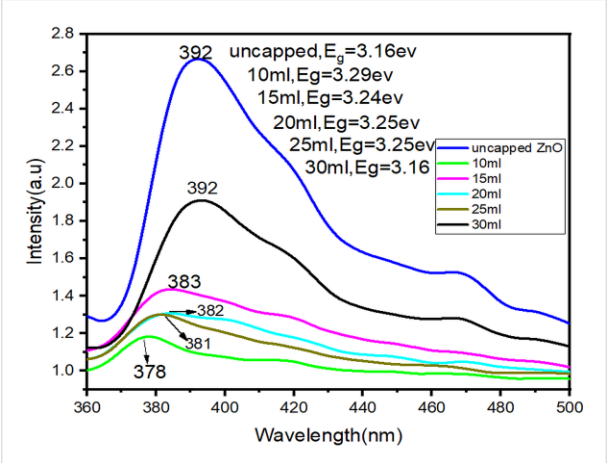

Figure 13: PL spectra of uncapped ZnO and the 10-30 mL extract series

All samples exhibit a dominant near-band-edge feature between 378 and 392 nm. Relative peak intensities were reported as 2.67 a.u. (0 mL), 1.18 a.u. (10 mL), 1.44 a.u. (15 mL), 1.32 a.u. (20 mL), 1.30 a.u. (25 mL), and 1.91 a.u. (30 mL). The lower intensity of most capped samples may reflect increased non-radiative surface transfer, reduced emitting-particle concentration, altered excitation absorption, or passivation of particular radiative defect channels. Because both quenching and enhancement can accompany passivation depending on the dominant pathway, the data should be described as evidence that extract concentration changes recombination behavior—not as a unique proof that one condition has fewer total defects.

The 15 mL sample does not have the lowest PL peak intensity, but it combines intermediate PL behavior with the most favorable reported XRD indicators. Thus, calling 15 mL "optimal" is best understood as a multi-criterion structural compromise rather than a universal optical optimum. The optimum could change for photocatalysis, gas sensing, antimicrobial activity, or light emission because each application values a different balance of surface area, defect chemistry, carrier lifetime, and agglomeration.

3.10 Integrated structure-surface-optical response

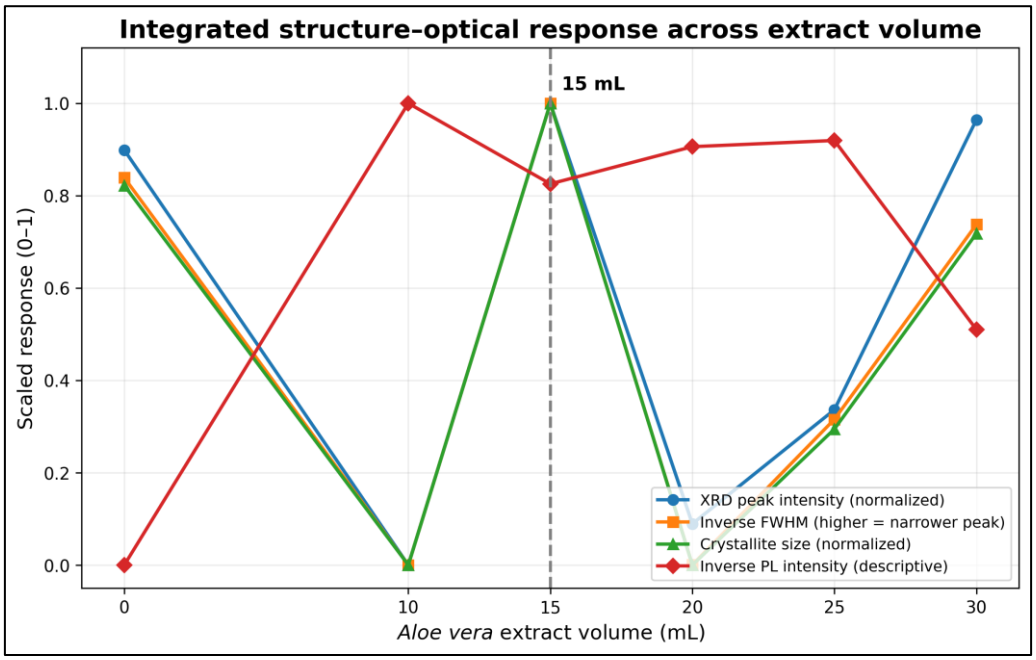

Figure 14: Integrated normalized response of reported structural and PL descriptors across extract concentration. Values were normalized to their within-series maxima for visualization only. The plot is descriptive, contains no replicate uncertainty, and should not be interpreted as a statistical optimization model

The integrated view highlights the non-monotonic nature of the system. At 15 mL, selected-peak intensity and Scherrer size are maximized while FWHM and the single-line strain proxy are minimized. At 30 mL, structural intensity and PL intensity rise again, which may indicate renewed particle ordering, aggregation, altered organic residue, or differences in sample loading. The available measurements support the practical choice of 15 mL for follow-up work, but mechanistic discrimination requires independent size and morphology measurements and replicated batches.

4. Mechanistic, Sustainability, and Application Perspective

4.1 Mechanistic interpretation across extract concentration

A coherent working model can be divided into three regimes. At low extract volume, limited macromolecular coverage may increase nucleation while incompletely stabilizing nascent particles, producing broader diffraction peaks and lower coherent-domain size. At an intermediate volume (15 mL in the current dataset), coordination and adsorption may regulate nucleation and growth sufficiently to improve structural order without strongly blocking crystallization. At higher volumes, excess soluble organics can increase solution viscosity, modify ion activity and local pH, occupy growth sites, or leave more residue; later calcination can remove or transform this material and permit secondary crystallite coarsening or aggregation. This model explains a non-monotonic response but remains a hypothesis until supported by time-resolved synthesis, composition, and morphology data.

4.2 What "green" should mean in this system

The use of an aqueous plant extract reduces reliance on synthetic capping ligands and is compatible with abundant renewable biomass. Nevertheless, sodium hydroxide, zinc acetate, ethanol washing, repeated centrifugation, overnight drying, and 350 °C calcination

contribute material, water, and energy burdens. A stronger sustainability claim would quantify atom economy or material efficiency, product yield, water and ethanol consumption, energy per gram of ZnO, extract-to-product ratio, waste pH, and the feasibility of solvent recovery. Comparison with a conventional precipitation control using the same thermal history is particularly important because "green" should describe improved process performance, not only the identity of one ingredient.

4.3 Potential applications and required validation

The measured near-UV optical response and tunable surface chemistry make the materials plausible candidates for UV-responsive coatings, photocatalytic interfaces, gas-sensing layers, and optoelectronic or luminescent components [1,2]. These are potential applications, not demonstrated performances. Photocatalysis would require kinetic tests with dark adsorption controls, photolysis controls, irradiance measurement, catalyst recovery, and cycling. Sensing would require sensitivity, selectivity, response/recovery time, humidity dependence, and long-term drift. Antimicrobial claims would require standardized organisms, dose metrics, particle-only and extract-only controls, dissolution measurements, and cytotoxicity assessment. Device-oriented claims would require film fabrication, electrical measurements, stability, and comparison with benchmark ZnO.

4.4 Minimum characterization for a publication-ready follow-up

Question	Recommended method	Why it matters
What are particle size and morphology?	SEM and TEM with blinded image analysis	Distinguishes particle size from XRD coherent-domain size and reveals aggregation/shape.
Is the material compositionally pure?	EDS/ICP-OES and XPS	Checks elemental composition, trace impurities, surface chemical states, and residual carbon.
How much organic matter remains?	TGA/DSC with evolved-gas analysis	Quantifies moisture and phytochemical residue after drying/calcination.
How stable are dispersions?	DLS, zeta potential, and time-dependent sedimentation	Evaluates hydrodynamic size, aggregation, and surface charge.
Are optical values reproducible?	Raw spectral export, replicate scans, baseline protocol, objective Tauc fitting	Provides uncertainty and prevents fit-window bias.
Does the proposed application work?	Application-specific benchmark and control experiments	Separates promising material descriptors from actual functional performance.

Note. Reporting should follow a minimum-information approach: complete material characterization, complete experimental protocols, raw/processed data availability, and clear distinction between independent replicates and repeated instrument scans [11].

5. Limitations and Data-Quality Considerations

- Independent synthesis replicates, standard deviations, confidence intervals, and statistical tests were not supplied; all concentration trends are therefore descriptive.
- Instrument models and acquisition parameters were incomplete, limiting assessment of XRD peak widths, FTIR comparability, UV-visible baseline behavior, and PL intensity normalization.
- The selected XRD peak near 38.2° was labeled (101), but standard Cu Kα wurtzite ZnO places (101) near 36.25°; raw files and indexing must be rechecked.
- The original capped/uncapped XRD table contained a likely decimal error in Scherrer size and inconsistent lattice parameters; corrected values in this revision must be verified from raw data.
- The concentration-series Tauc intercepts of 5.6-6.2 eV conflict with the 370-400 nm absorption edges and 378-392 nm PL; they must not be treated as intrinsic band gaps.
- No SEM/TEM, elemental analysis, surface-area measurement, XPS, DLS, zeta potential, TGA, or yield data were available, so morphology, chemical purity, surface coverage, aggregation, and process efficiency remain unresolved.
- No photocatalytic, sensing, antimicrobial, electrical, or device tests were performed; application statements are prospective.

These limitations do not invalidate the observed spectral and diffraction trends. Instead, they define the boundary between a useful preliminary concentration-screening study and a fully validated structure-property investigation suitable for a high-impact materials journal.

6. CONCLUSIONS

ZnO nanoparticles were produced by alkaline precipitation using Aloe vera inner-leaf gel as a plant-derived complexing, nucleation-regulating, and surface-capping medium. The extract volume generated a non-monotonic response across XRD, FTIR, UV-visible, and PL measurements. All reported diffraction patterns were broadly consistent with wurtzite ZnO and showed no obvious additional crystalline phase. Within the available concentration series, 15 mL gave the strongest combined structural indicators: selected-peak intensity of 2067 a.u., FWHM of 0.49327°, Scherrer coherent-

domain size of 17.05 nm, and the lowest single-line strain estimate of 0.00620. FTIR spectra supported Zn-O formation and the presence of extract-derived surface functional groups. Near-UV absorption and near-band-edge PL at 378-392 nm were compatible with ZnO optical energies of approximately 3.16-3.29 eV.

A major outcome of the critical revision is the recognition that the reported concentration-series Tauc intercepts of 5.6-6.2 eV are inconsistent with the spectra and should be recalculated rather than rationalized as extreme quantum confinement. The study therefore supports 15 mL as the most balanced condition for follow-up synthesis, not as a statistically proven universal optimum. Replicated batches, raw-data reanalysis, full-pattern XRD refinement, microscopy, compositional and surface characterization, colloidal measurements, and application-specific testing are required to convert the preliminary structure-optical correlation into a reproducible and technologically meaningful material platform.

DECLARATIONS

Conflict of interest

The authors declare that they have no known competing financial interests or personal relationships that could have appeared to influence the work reported in this paper.

Data availability

The raw XRD, FTIR, UV-visible, and photoluminescence data files and analysis scripts were not included with the supplied manuscript. For publication, the authors should deposit raw and processed datasets, sample metadata, and fitting procedures in a stable repository or make them available as supplementary information.

Author contributions

A CRediT author-contribution statement should be completed after the final author list is confirmed. Do not assign contributions that cannot be verified.

Highlights

- Aloe vera inner-gel extract was evaluated as a concentration-dependent complexing, nucleation-regulating, and capping medium for ZnO formation.
- The 15 mL condition gave the strongest reported structural indicators: 2067 a.u. selected-peak intensity, 0.49327° FWHM, 17.05 nm crystallite size, and 0.00620 single-line strain.
- Zn-O vibrations and extract-derived functional groups support formation of phytochemical-associated ZnO surfaces.
- Near-UV absorption and 378-392 nm emission support an optical transition near 3.1-3.3 eV; 5.6-6.2 eV Tauc intercepts are flagged as non-physical apparent values.
- The revised interpretation separates measured evidence from proposed mechanisms and defines the data required for reproducible, application-ready validation.

REFERENCES

1. R. Raha and M. Ahmaruzzaman, "ZnO nanostructured materials and their potential applications: progress, challenges and perspectives," Nanoscale Advances, vol. 4, pp. 1868-1925, 2022. doi: 10.1039/D1NA00880C.
2. G. Sangeetha, S. Rajeshwari, and R. Venckatesh, "Green synthesis of zinc oxide nanoparticles by Aloe barbadensis Miller leaf extract: structure and optical properties," Materials Research Bulletin, vol. 46, no. 12, pp. 2560-2566, 2011. doi: 10.1016/j.materresbull.2011.07.046.
3. N. I. Rasli, H. Basri, and Z. Harun, "Zinc oxide from Aloe vera extract: two-level factorial screening of biosynthesis parameters," Heliyon, vol. 6, e03156, 2020. doi: 10.1016/j.heliyon.2020.e03156.
4. S. Ahmed, S. A. Chaudhry, and S. Ikram, "A review on biogenic synthesis of ZnO nanoparticles using plant extracts and microbes: a prospect towards green chemistry," Journal of Photochemistry and Photobiology B: Biology, vol. 166, pp. 272-284, 2017. doi: 10.1016/j.jphotobiol.2016.12.011.
5. J. H. Hamman, "Composition and applications of Aloe vera leaf gel," Molecules, vol. 13, no. 8, pp. 1599-1616, 2008. doi: 10.3390/molecules13081599.
6. B. D. Viezbicke, S. Patel, B. E. Davis, and D. P. Birnie III, "Evaluation of the Tauc method for optical absorption edge determination: ZnO thin films as a model system," physica status solidi (b), vol. 252, no. 8, pp. 1700-1710, 2015. doi: 10.1002/pssb.201552007.
7. A. Makuła, M. Pacia, and W. Macyk, "How to correctly determine the band gap energy of modified semiconductor photocatalysts based on UV-Vis spectra," The Journal of Physical Chemistry Letters, vol. 9, no. 23, pp. 6814-6817, 2018. doi: 10.1021/acs.jpclett.8b02892.
8. Y. Feng, S. Lin, S. Huang, S. Shrestha, and G. Conibeer, "Can Tauc plot extrapolation be used for direct-band-gap semiconductor nanocrystals?," Journal of Applied Physics, vol. 117, no. 12, 125701, 2015. doi: 10.1063/1.4916090.
9. H. E. Swanson and E. Tatge, Standard X-ray Diffraction Powder Patterns, National Bureau of Standards Circular 539, vol. 2. Washington, DC: U.S. Department of Commerce, 1953.
10. M. D. McCluskey and S. J. Jokela, "Defects in ZnO," Journal of Applied Physics, vol. 106, 071101, 2009. doi: 10.1063/1.3216464.
11. M. Faria *et al.,* "Minimum information reporting in bio-nano experimental literature," Nature Nanotechnology, vol. 13, pp. 777-785, 2018. doi: 10.1038/s41565-018-0246-4.

12. S. Talam, S. R. Karumuri, and N. Gunnam, "Synthesis, characterization, and spectroscopic properties of ZnO nanoparticles," International Scholarly Research Notices, vol. 2012, 372505, 2012. doi: 10.5402/2012/372505.
13. S. Singh, J. V. Gade, D. K. Verma, B. Elyor, and B. Jain, "Exploring ZnO nanoparticles: UV-visible analysis and different size estimation methods," Optical Materials, vol. 152, 115422, 2024. doi: 10.1016/j.optmat.2024.115422.
14. S. S. Zak, W. H. A. Majid, M. E. Abrishami, and R. Yousefi, "X-ray analysis of ZnO nanoparticles by Williamson-Hall and size-strain plot methods," Solid State Sciences, vol. 13, no. 1, pp. 251-256, 2011. doi: 10.1016/j.solidstatesciences.2010.11.024.
15. G. K. Williamson and W. H. Hall, "X-ray line broadening from filed aluminium and wolfram," Acta Metallurgica, vol. 1, no. 1, pp. 22-31, 1953. doi: 10.1016/0001-6160(53)90006-6.
16. M. T. El-Saadony *et al.,* "Green Synthesis of Zinc Oxide Nanoparticles: Preparation, Characterization, and Biomedical Applications—A Review," International Journal of Nanomedicine, vol. 19, pp. 12889-12937, 2024. doi: 10.2147/IJN.S487188.